A Physics-based Model for PEMFCs: Process Identification from EIS Simulation

Georg Futter[1], Arnulf Latz[1,2], Thomas Jahnke[1]

1: German Aerospace Center (DLR), Stuttgart, Germany

2: Helmholtz Institute Ulm for Electrochemical Energy Storage (HIU), Ulm, Germany

Motivation

Why physical modeling of fuel cells?

- Better understanding of processes in the cell and their interaction
- Insights on experimentally inaccessible properties
- Simulation based prediction of cell performance and lifetime
- Optimization of cell performance and durability

Challenges:

- Complex system: coupling of processes on very different time and length scales
- Details of the involved mechanisms often unknown and material dependent
- Heterogeneities within the cell require 2D and 3D cell models

Modeling approach

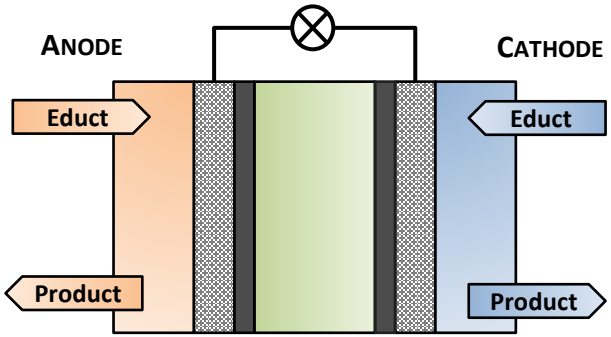

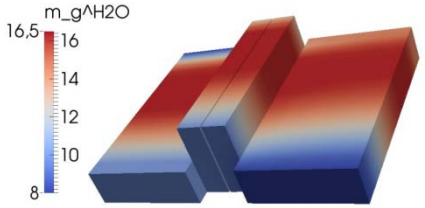

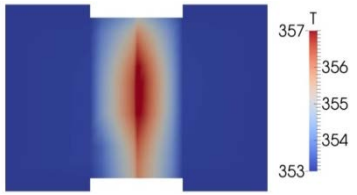

Multi-scale cell models

Model validation

Degradation models

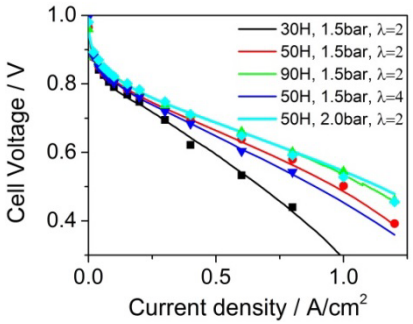

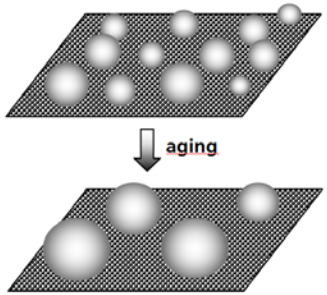

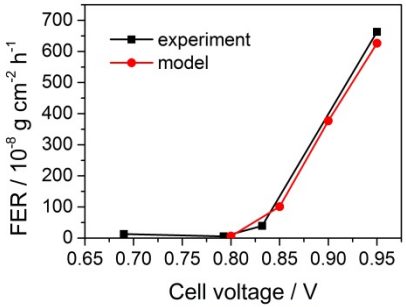

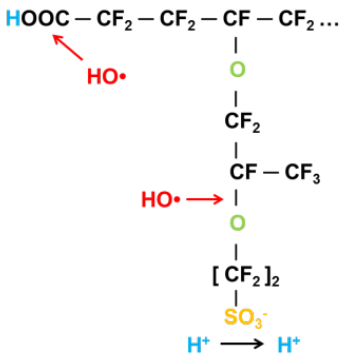

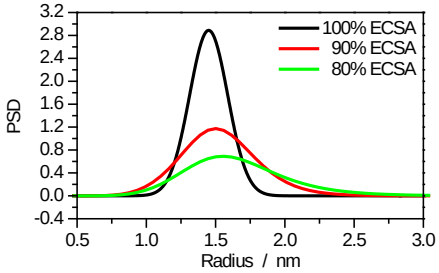

Framework

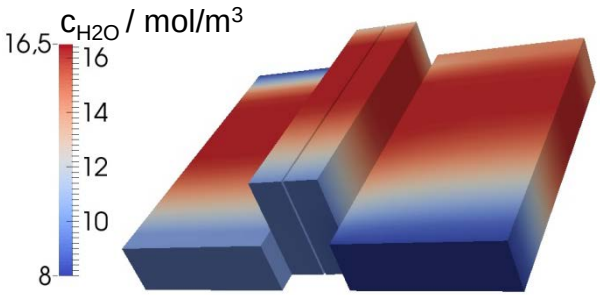

Generic framework for the simulation of multi-phase flow and transport in porous media

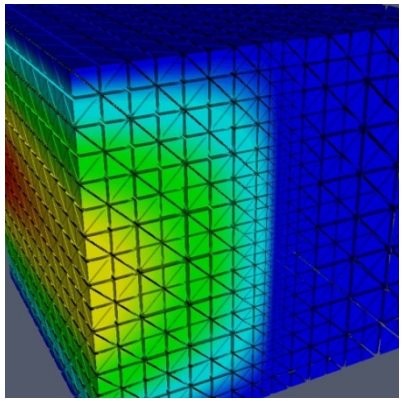

Neopard.FC/EL

Dumux

DUNE

Framework to investigate performance and degradation of fuel cells and electrolyzers via transient 2D and 3D simulations

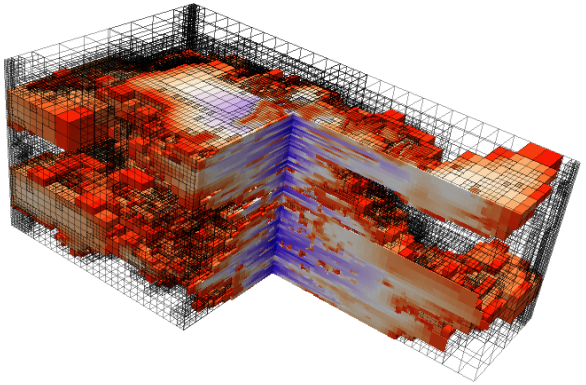

Modular toolbox for solving partial differential equations (PDEs) with grid-based methods

NEOPARD-FC/EL: Numerical Environment for the Optimization of Performance And Reduction of Degradation of Fuel Cells/ELectrolyzers

- Developed at DLR since 2013

NEOPARD-FC features

- 2D and 3D discretizations of the cells
- Transport models for the cell components
- Electrochemistry models
- Specific fluid systems for the different technologies
- Transient simulations (e.g. EIS)
- Models for degradation mechanisms

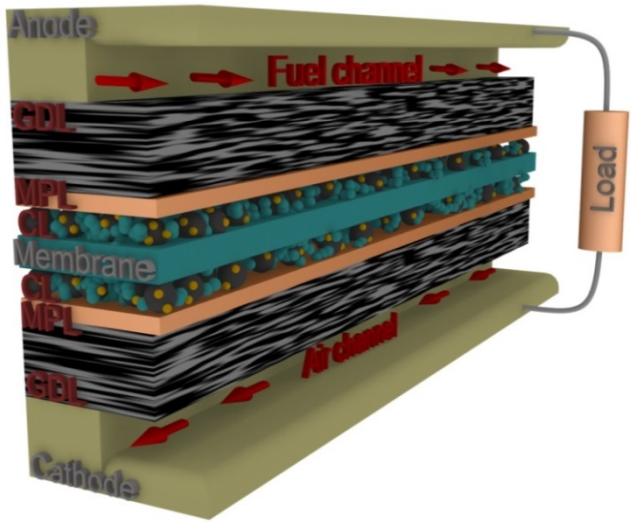

Field of Application:

- PEMFC
- DMFC
- SOEC

PEMFC model features

- 9 layers spatially resolved (channels, GDLs, MPLs, CLs, MEM)
- Two-phase multi-component transport model
- Charge transport in ionomer phase
- Ionomer film model
- ORR: BV kinetics with doubling of Tafel slope
- Platinum oxide model
- Gas crossover through membrane
- Non-isothermal
- Realistic boundary conditions: lambda-control at fixed back pressure in potentiostatic and galvanostatic mode

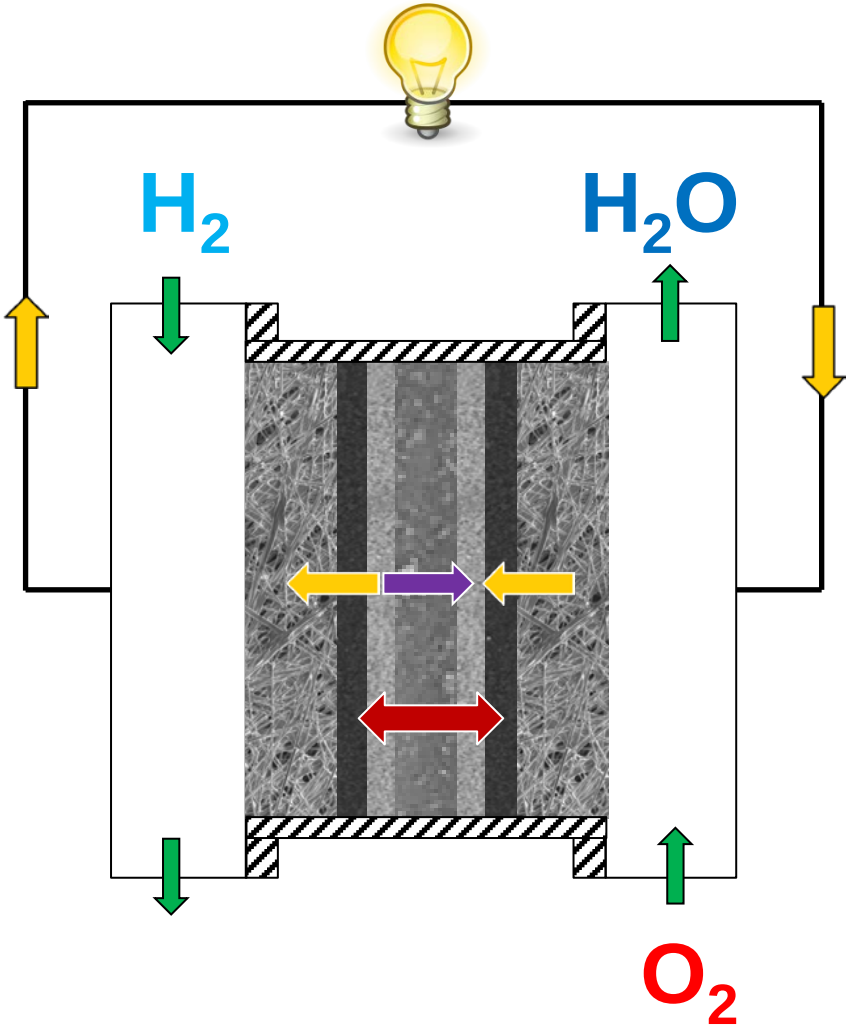

Two-phase transport model

- Multiphase Darcy approach + nonlinear complementarity function for robust treatment of phase transitions[1]
  - Arbitrary number of phases → here: gas + liquid
  - Arbitrary number of components

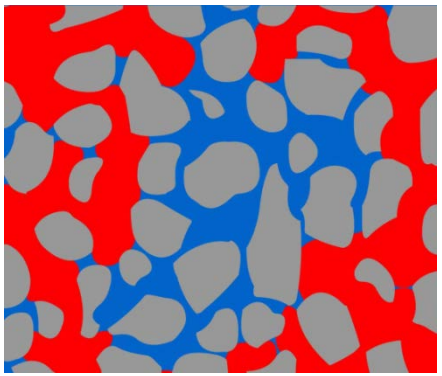

$$\frac{\partial \xi^{\kappa}}{\partial t} + \nabla \cdot \Psi^{\kappa} - q^{\kappa} = 0; \qquad \xi^{\kappa} = \phi \sum_{\alpha=1}^{M} \rho_{mol,\alpha} x_{\alpha}^{\kappa} S_{\alpha}$$

$$\Psi^{\kappa} = \sum_{\alpha=1}^{M} \left(\frac{k_{r,\alpha}}{\mu_{\alpha}} \rho_{mol,\alpha} x_{\alpha}^{\kappa} K \nabla p_{\alpha} + D_{pm,\alpha}^{\kappa} \rho_{mol,\alpha} \nabla x_{\alpha}^{\kappa} \right)$$

- Knudsen diffusion in gas phase

$$D_{pm,g}^{\kappa} = \left(S_g \phi\right)^{1.5} \left(\frac{1}{D_{Knudsen}^{\kappa}} + \frac{1}{\tilde{D}_g^{k}} \right)^{-1}; \qquad D_{Knudsen}^{\kappa} = r \frac{2}{3} \sqrt{\frac{8RT}{\pi M^{k}}}$$

[1]: Lauser et al., **2011**, *Adv. Water Resour.*, *34*(8).

Transport in the Polymer Electrolyte Membrane

Weber-Newman model[1]:

$$\frac{\partial \xi}{\partial t} + \nabla \cdot \Psi = 0$$

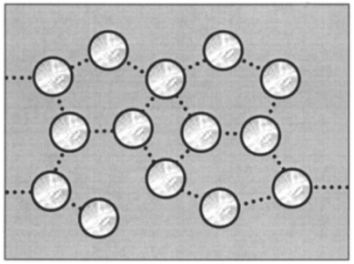

Vapor equilibrated

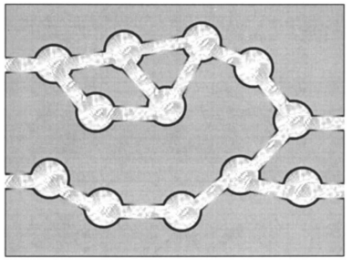

Liquid equilibrated

- **H^+:**

$$\Psi = S\left(-\sigma\nabla\Phi - \frac{\sigma n_{drag,l}}{F}\nabla\mu_{H_2O}\right) + (1-S)\left(-\sigma\nabla\Phi - \frac{\sigma n_{drag,v}}{F}\nabla\mu_{H_2O}\right)$$

- **H_2O:**

$$\Psi = S\left(-\frac{\sigma n_{drag,l}}{F}\nabla\Phi - \left(\alpha_l + \frac{\sigma n_{drag,l}^2}{F^2}\right)\nabla\mu_{H_2O}\right) + (1-S)\left(-\frac{\sigma n_{drag,v}}{F}\nabla\Phi - \left(\alpha_v + \frac{\sigma n_{drag,v}^2}{F^2}\right)\nabla\mu_{H_2O}\right)$$

- **Gas species (O_2, H_2):**

$$\Psi^k = -\psi^k \nabla p^k$$

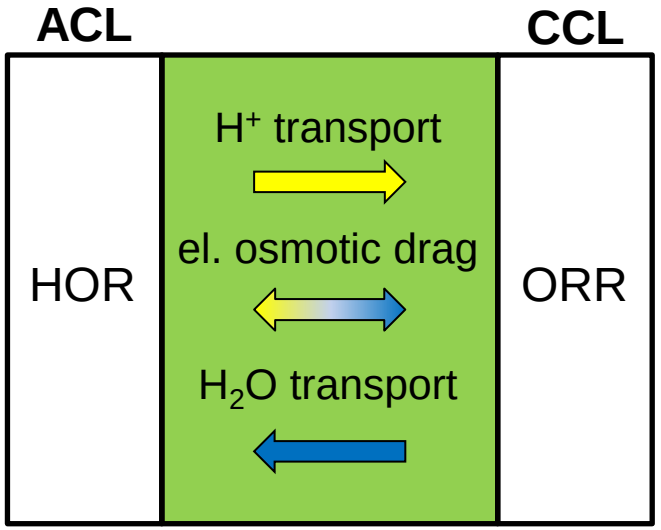

[1]: Weber, Newman, **2004**, *J. Electrochem. Soc.*, 151(2).

Electronic and Ionic Charge Balance in the Electrodes

- Electron transport in the BPPs, GDLs, MPLs, CL:

$$-\frac{\partial C_{DL}\left(\Phi_{elde}-\Phi_{elyte}\right)}{\partial t}+\nabla\cdot\left(\sigma_{eff}^{e^-}\nabla\Phi_{elde}\right)-q^{e^-}=0$$

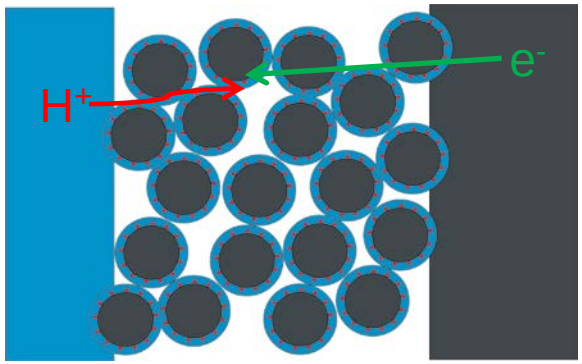

- Proton transport in the CLs:

$$-\frac{\partial C_{DL}\left(\Phi_{elde}-\Phi_{elyte}\right)}{\partial t}+\nabla\cdot\left(-\sigma_{eff}^{H^+}\nabla\Phi_{elyte}\right)-q^{H^+}=0$$

- Ionic conductivity strongly depends on RH [1,2]

$$\sigma_{eff}^{H^+}=\sigma^{H^+}\left(a_{H2O}\right)$$

[1]: D. K. Paul et al., JES, 161 (**2014)** F1395.
[2]: B. P. Setzler, F. Fuller JES, 162 (**2015)** F519.

Ionomer film model

- Model for ORR reaction rate taking into account
  - Oxygen transport through ionomer film
  - Resistances at gas/ionomer and ionomer/Pt interfaces[1]

- Analytical solutions are possible for $r_{BV} \propto c_{O2}$ and $r_{BV} \propto \sqrt{c_{O2}}$

- Reaction rate for $r_{BV} \propto \sqrt{c_{O2}}$:

$$r = \frac{\sqrt{4A_{eff} n^2 F^2 c_{O2} + R^2 k^2} - Rk}{2A_{eff} nF} k$$

$$k = ECSA\ i_o c_{ref}^{-0.5} \left[\exp\left(\frac{\alpha nF\eta}{RT} \right) - \exp\left(\frac{(1-\alpha) nF\eta}{RT} \right) \right]$$

$$R = \frac{\delta_{ion}}{D_{O2,ion}} + R_{\text{int}}\left(a_{H2O}\right)$$

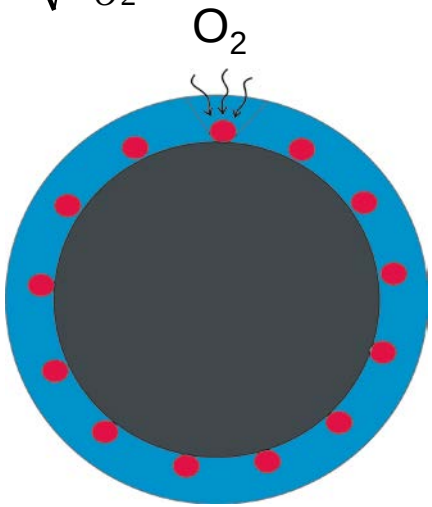

[1]: Hao et al., JES, 162 (**2015)** F854.

Model validation

- Model validation under various operating conditions is important for reliability
  - Different RH

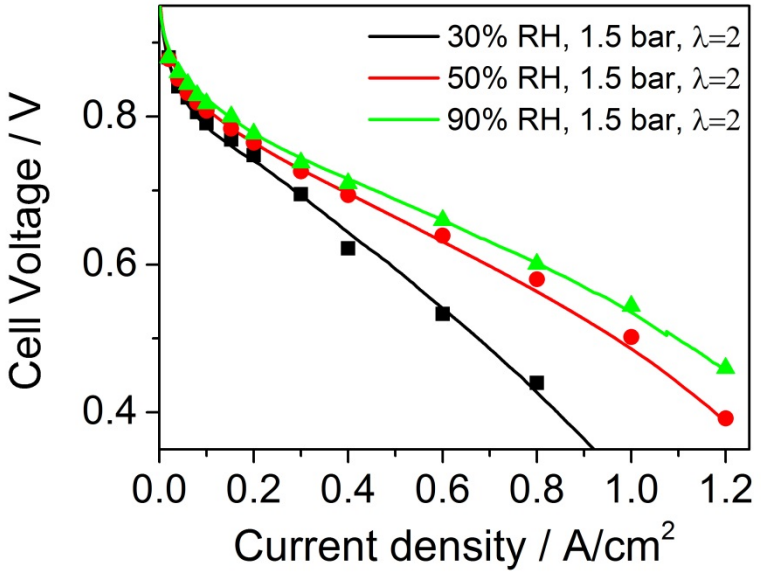

- Strong effect of RH on cell performance (Tafel slope + transport)

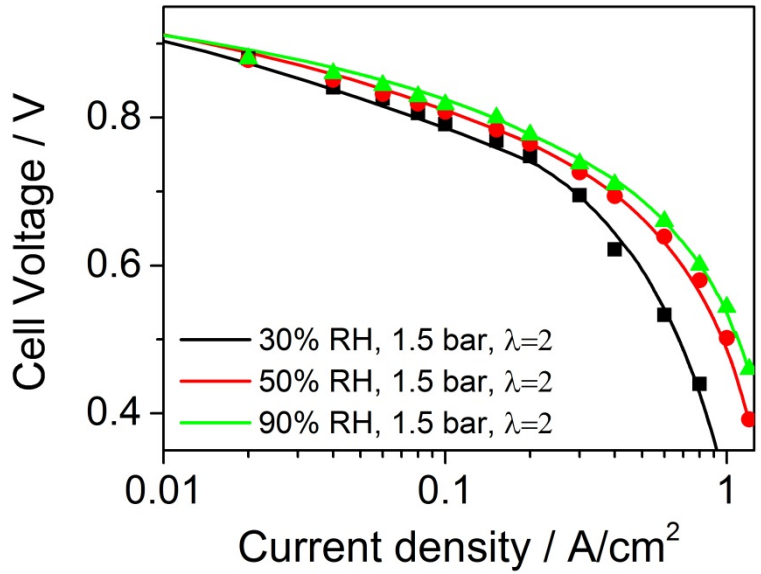

Model validation

- Model validation under various operating conditions is important for reliability
  - Different RH
  - Different pressure

- Strong effect of RH on cell performance (Tafel slope + transport)

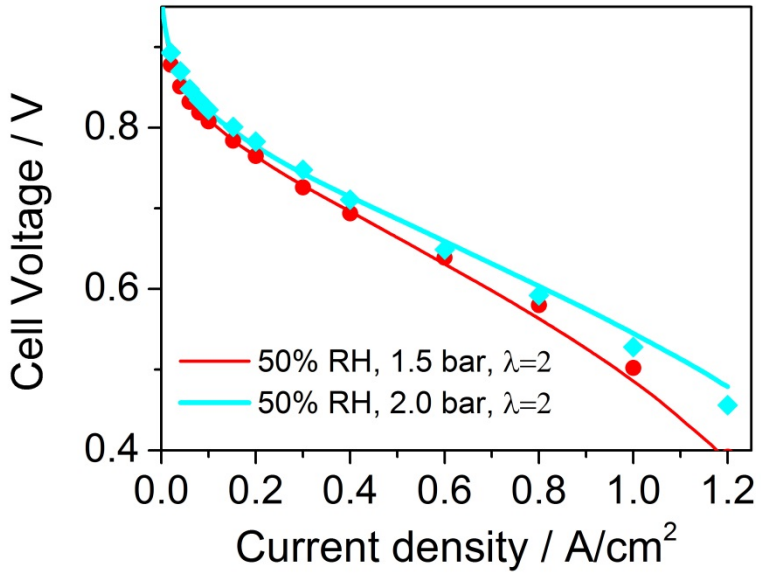

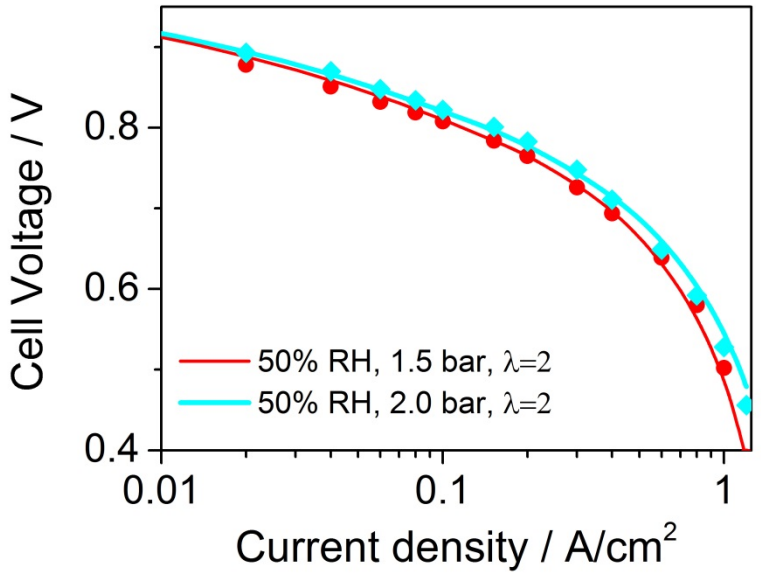

Model validation

- Model validation under various operating conditions is important for reliability
  - Different RH
  - Different pressure
  - Different stoichiometry

- Strong effect of RH on cell performance (Tafel slope + transport)
- High stoichiometry at 50% leads to lower performance → drying out overcompensates higher oxygen partial pressure

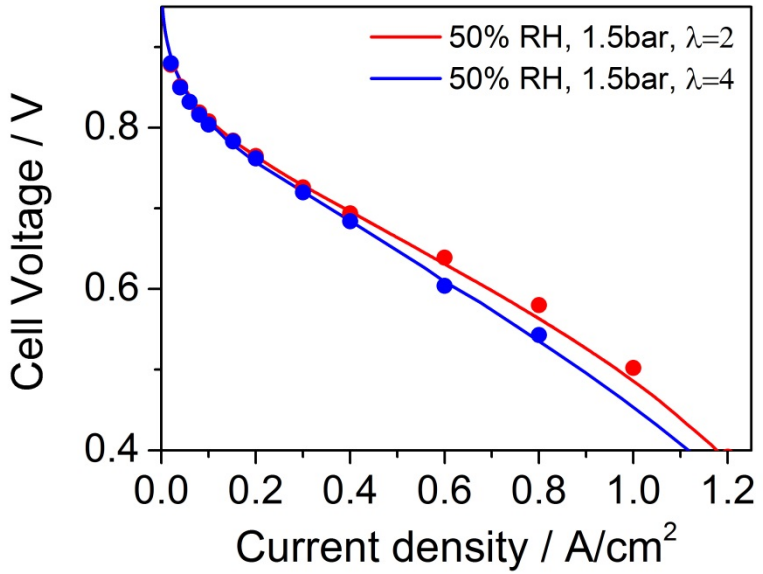

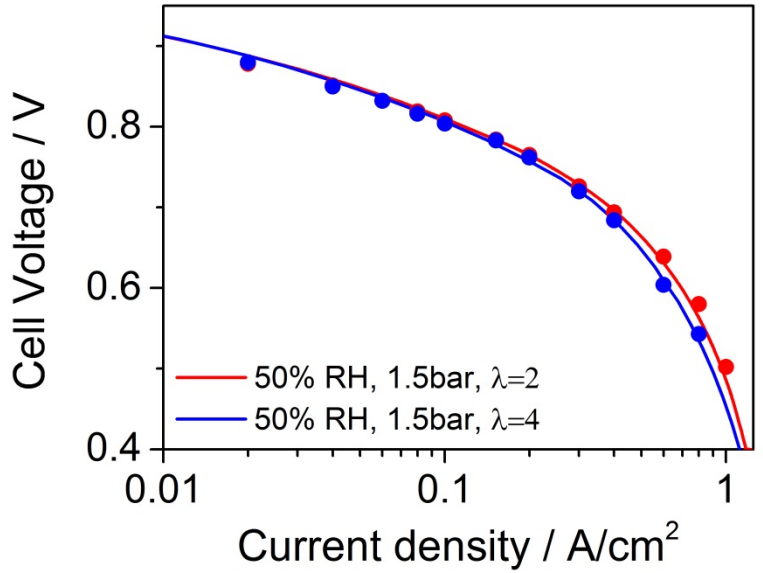

Model validation

- Model validation under various operating conditions is important for reliability
  - Different RH
  - Different pressure
  - Different stoichiometry

- Strong effect of RH on cell performance (Tafel slope + transport)
- High stoichiometry at 50% leads to lower performance → drying out overcompensates higher oxygen partial pressure
- 50% RH at 2 bar shows similar performance to 90% RH at 1.5 bar

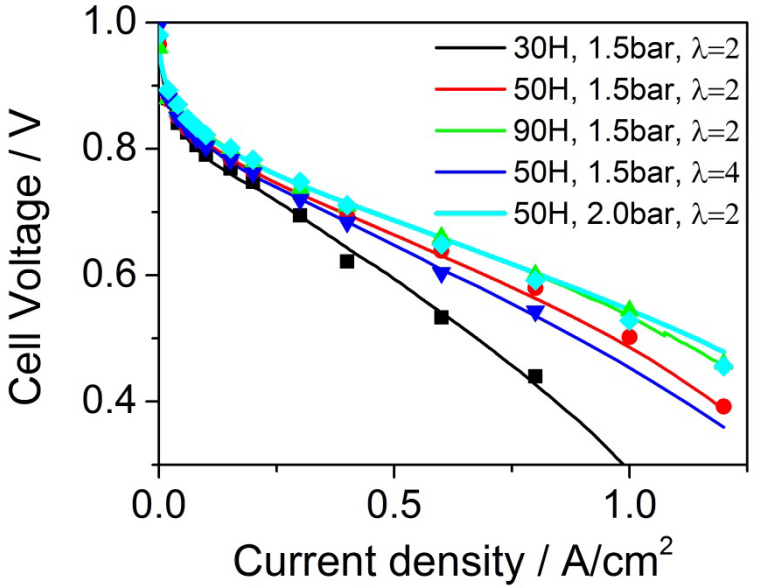

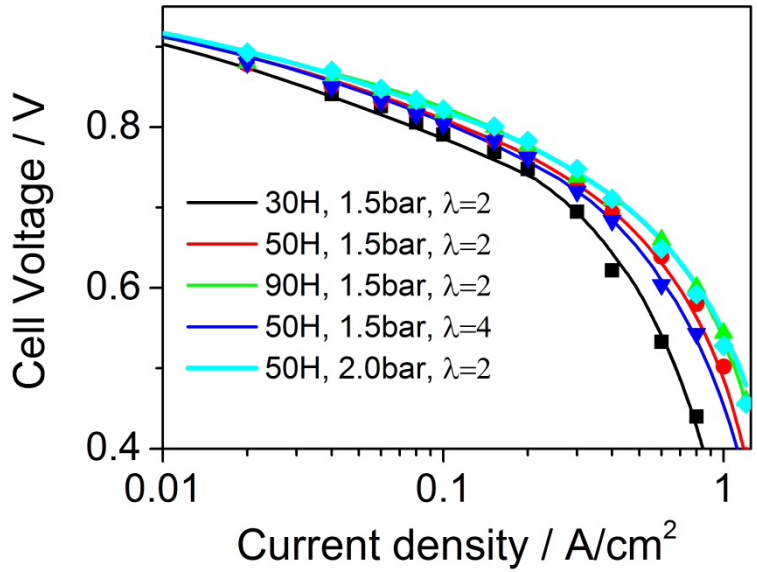

Model validation

Impedance measurements at various current densities for 30% RH and 50% RH:

- Trends and frequencies are correctly described by the model
- Total values still show a significant deviation

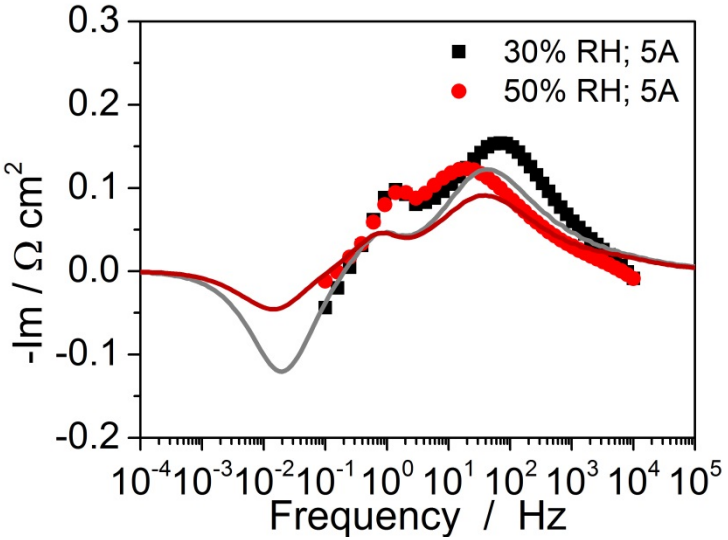

- RH affects proton conductivity and gas transport through ionomer
- Inductive feature at low frequency can explain the difference between low frequency resistance and slope of iV-curve
  - ➢Ionic conductivity in CLs
  - ➢PtOx coverage
  - ➢Thermal effects

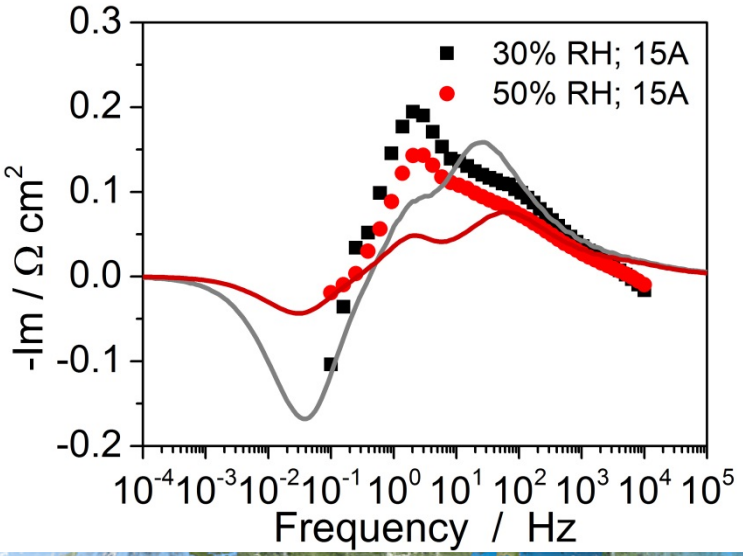

Cathode catalyst utilization

ORR reaction rate distribution

- Location of maximum reaction rate and distribution strongly depends on operating conditions
- At high RH
  - Very homogeneous at low current densities
- At low RH
  - Strong heterogeneities along channel
  - A significant part of the CCL is not used

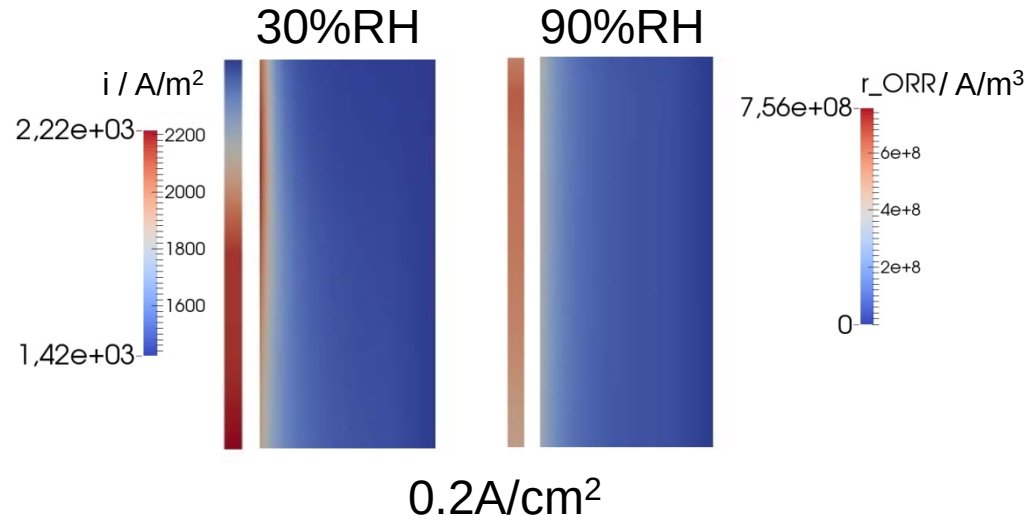

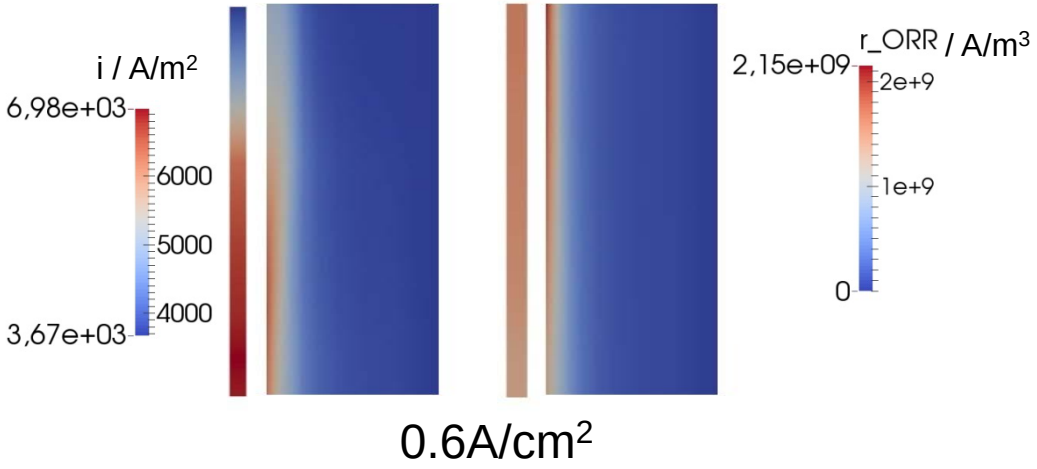

Chemical Membrane Degradation

Nr.	Reaction	k (M^{-1} s^{-1})	E_{act} (kJ mol^{-1})
1	$Fe^{2+} + H_2O_2 + H^+ \rightarrow Fe^{3+} + HO\bullet + H_2O$	65	35.4
2	$Fe^{3+} + H_2O_2 \rightarrow Fe^{2+} + HOO\bullet + H^+$	$7 \cdot 10^{-4}$	126
3	$Fe^{2+} + HOO\bullet + H^+ \rightarrow Fe^{3+} + H_2O_2$	$1.2 \cdot 10^{6}$	42
4	$Fe^{3+} + HOO\bullet \rightarrow Fe^{2+} + O_2 + H^+$	$2 \cdot 10^{4}$	33
5	$HO\bullet + H_2O_2 \rightarrow HOO\bullet + H_2O$	$2.7 \cdot 10^{7}$	14
6	$HOO\bullet + H_2O_2 \rightarrow HO\bullet + H_2O + O_2$	3	30
7	$2HOO\bullet \rightarrow H_2O_2 + O_2$	$8.6 \cdot 10^{5}$ (s^{-1})	20.6
8	$HO\bullet + H_2 \rightarrow H\bullet + H_2O$	$4.2 \cdot 10^{7}$	???
9	$H\bullet + O_2 \rightarrow HOO\bullet$	$2.1 \cdot 10^{10}$	???

$$Fe^{3+} + e^- \rightarrow Fe^{2+}$$

$$O_2 + 2H^+ + 2e^- \rightarrow H_2O_2$$

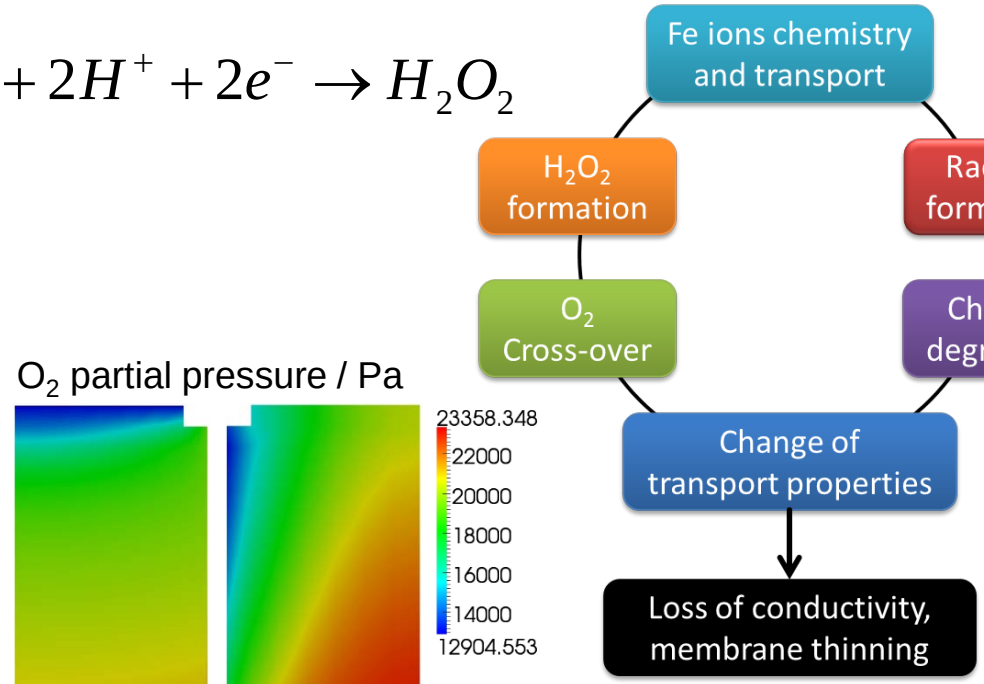

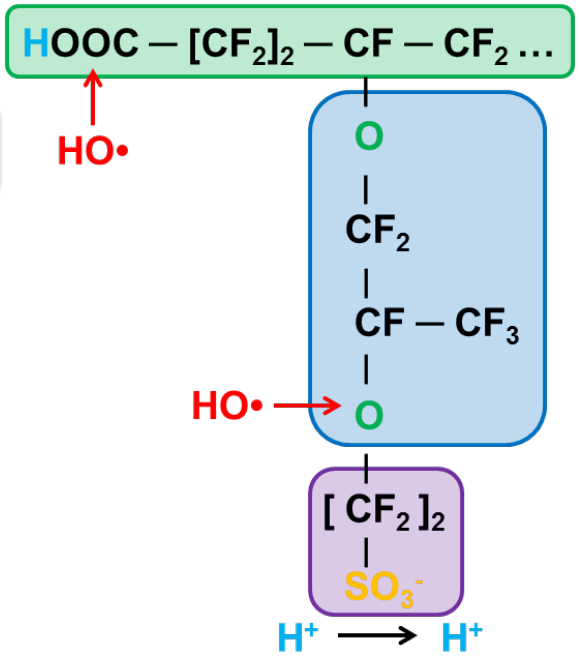

[1]: Wong & Kjeang, **2015**, Chem. Sus. Chem. 8(6).

Chemical Membrane Degradation

- O_2 crossover governs the H_2O_2 formation at the anode → maximum concentration on anode side at the cathode inlet
- At OCV: small gradients in electrolyte potential → ions move due to concentration gradients
- Overpotential for reduction is highest at the anode
- At 0.8V: Increasing gradients in electrolyte potential drag the ions to the cathode side → Degradation ceases

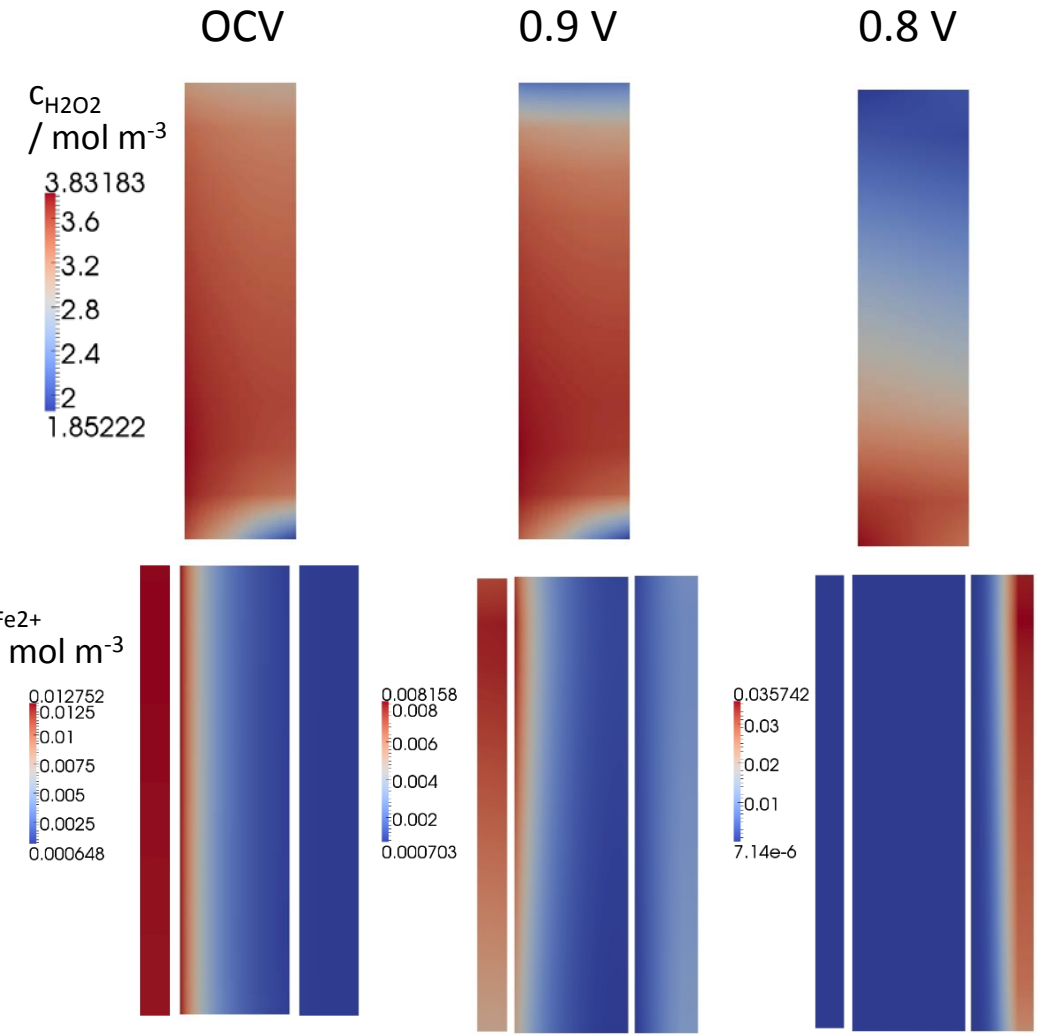

Chemical Membrane Degradation

- At OCV: Combination of H_2O_2 formation and transport with the Fe redox cycle leads to high degradation rate at the ACL / PEM interface until reinforcement layer → consistent with experimental results
- Decreasing cell potential results in strongly reduced degradation
- Simulated fluorine emission rates are in good agreement with experimental data

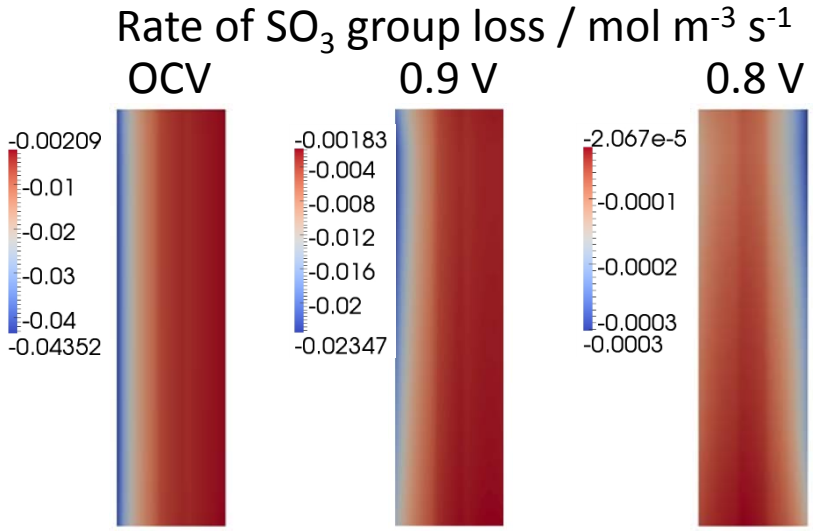

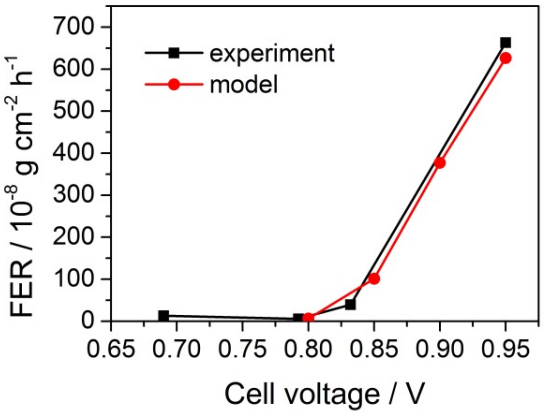

Fluorine emission rate (FER) @ 95 °C, pAnode=2.5 bar, pCathode=2.3 bar, RH=75%
(experiments provided by CEA)

Summary

- The development of predictive fuel cell models is challenging:
  - Complex interplay of many mechanisms on various time and length scales
  - Strong gradients within the cell require the development of 2D and 3D models
  - Model validation has to be performed under various operating conditions, ideally including the simulation of impedances to ensure model reliability

- Current density distribution strongly depends on the operating conditions
- At low relative humidity only a small fraction of the CL is used

- Chemical degradation of the membrane in PEMFC proceeds in several steps: Oxygen crossover from cathode to anode → Hydrogen peroxide formation → Radical formation → Radical attack of the membrane
- Amount and location of membrane degradation strongly depends on the cell potential. Highest degradation during OCV at anode side.

"It can scarcely be denied that the supreme goal of all theory is to make the irreducible basic elements as simple and as few as possible without having to surrender the adequate representation of a single datum of experience“

Albert Einstein

Thank you for your attention

The research leading to these results has received funding from the European Union's Seventh Framework Program (FP7/2007-2013) for the Fuel Cells and Hydrogen Joint Technology Initiative under grant agreement n°256776, n°.303419 and n°621216

Premium Act

Puma mind

Second Act

DLR

Transport and Performance Model: Gases and Liquid

Two-phase transport of gases and liquid

NCP-equations for phase transitions[1]

- If a phase is not present:

$$\forall \alpha : S_\alpha = 0 \rightarrow \sum_{\kappa=1}^{N} x_\alpha^\kappa \leq 1 \quad (1)$$

- If a phase is present

$$\forall \alpha : \sum_{\kappa=1}^{N} x_\alpha^\kappa = 1 \rightarrow S_\alpha \geq 0 \quad (2)$$

→ $$\forall \alpha : S_\alpha \left(1 - \sum_{\kappa=1}^{N} x_\alpha^\kappa \right) = 0 \quad (3)$$

- Equations 1-3 constitute a non-linear complementarity problem
- Solution is a non-linear complementarity function:

$$\Phi(a,b) = 0$$

$$a \geq 0 \wedge b \geq 0 \wedge a \cdot b = 0$$

$$\Phi(a,b) = \min\left\{ S_\alpha, 1 - \sum_{\kappa=1}^{N} x_\alpha^\kappa \right\}$$

[1]: Lauser et al., **2011**, *Adv. Water Resour.*, *34*(8).

Model Coupling and Schroeder's Paradox

Numerical Coupling:
- Dirichlet-Neumann

Physical Coupling:
- Macroscopic Approach**:**
- Local thermodynamic equilibrium

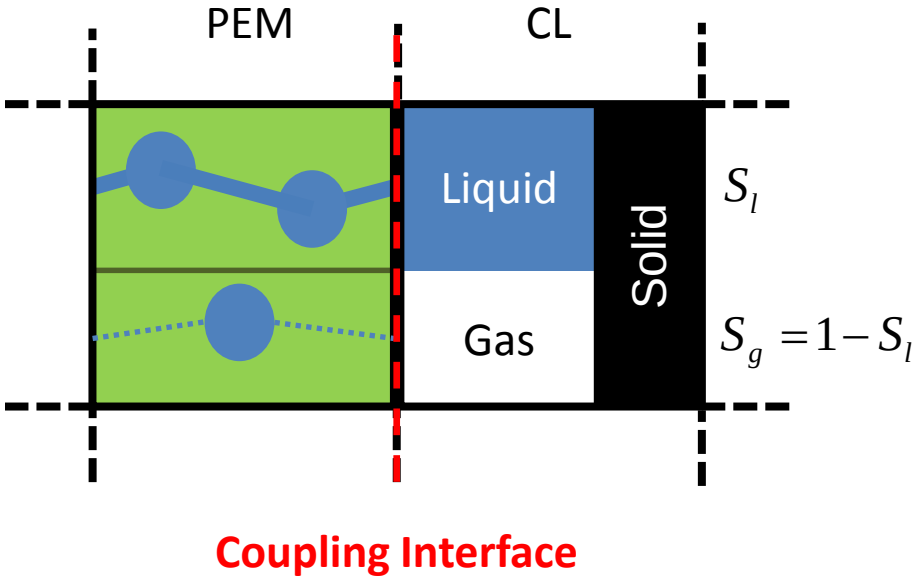

$$\lambda_l \approx 22$$

$$\lambda_g = f\left(a_{H_2O}\right)$$

$$\lambda_{PEM} = S_g \lambda_g + S_l \lambda_l$$

Chemical Degradation Model

Fe redox cycle and transport

- Electrochemical reaction:

$$Fe^{3+} + e^- \rightarrow Fe^{2+} \qquad E_0 = 0.77 + \ln\left(\frac{c_{Fe^{3+}}}{c_{Fe^{2+}}}\right)$$

$$r = akF\sqrt{c_{Fe^{2+}} c_{Fe^{3+}}}\left[\exp\left(\frac{F\eta}{2RT}\right) - \exp\left(\frac{-F\eta}{2RT}\right)\right]$$

- Description of ion transport in the membrane with generalized Nernst-Planck type equation[1]:

$$J_i = -D_i \nabla c_i - u_i z_i c_i F \nabla \Phi_{elyte} \qquad D_i = f_i u_i RT \qquad f_{Na^+} = 0.36 \text{ [1]}$$

Value for bi/trivalent ions is expected to be lower:

$$f_{Fe^{2/3+}} = 0.025$$

[1]: Auclair et al., **2002**, *J. Memb. Sci.*, 195, 89–102.

Radical Formation Reactions

Nr.	Reaction	k (M^{-1} s^{-1})	E_{act} (kJ mol^{-1})	
1	$Fe^{2+} + H_2O_2 + H^+ \rightarrow Fe^{3+} + HO\bullet + H_2O$	65	35.4	[1]
2	$Fe^{3+} + H_2O_2 \rightarrow Fe^{2+} + HOO\bullet + H^+$	$7 \cdot 10^{-4}$	126	
3	$Fe^{2+} + HOO\bullet + H^+ \rightarrow Fe^{3+} + H_2O_2$	$1.2 \cdot 10^{6}$	42	
4	$Fe^{3+} + HOO\bullet \rightarrow Fe^{2+} + O_2 + H^+$	$2 \cdot 10^{4}$	33	
5	$HO\bullet + H_2O_2 \rightarrow HOO\bullet + H_2O$	$2.7 \cdot 10^{7}$	14	
6	$HOO\bullet + H_2O_2 \rightarrow HO\bullet + H_2O + O_2$	3	30	
7	$2HOO\bullet \rightarrow H_2O_2 + O_2$	$8.6 \cdot 10^{5}$ (s^{-1})	20.6	
8	$HO\bullet + H_2 \rightarrow H\bullet + H_2O$	$4.2 \cdot 10^{7}$	???	[2]
9	$H\bullet + O_2 \rightarrow HOO\bullet$	$2.1 \cdot 10^{10}$	???	

[1]: Ghelichi et al., **2014**, *J. Phys. Chem. B*, 118(38).
[2]: Gubler et al., **2011**, *J. Electrochem. Soc.*, 158(7).

DLR

Degradation Mechanisms: Side-chain Cutting and Unzipping[1]

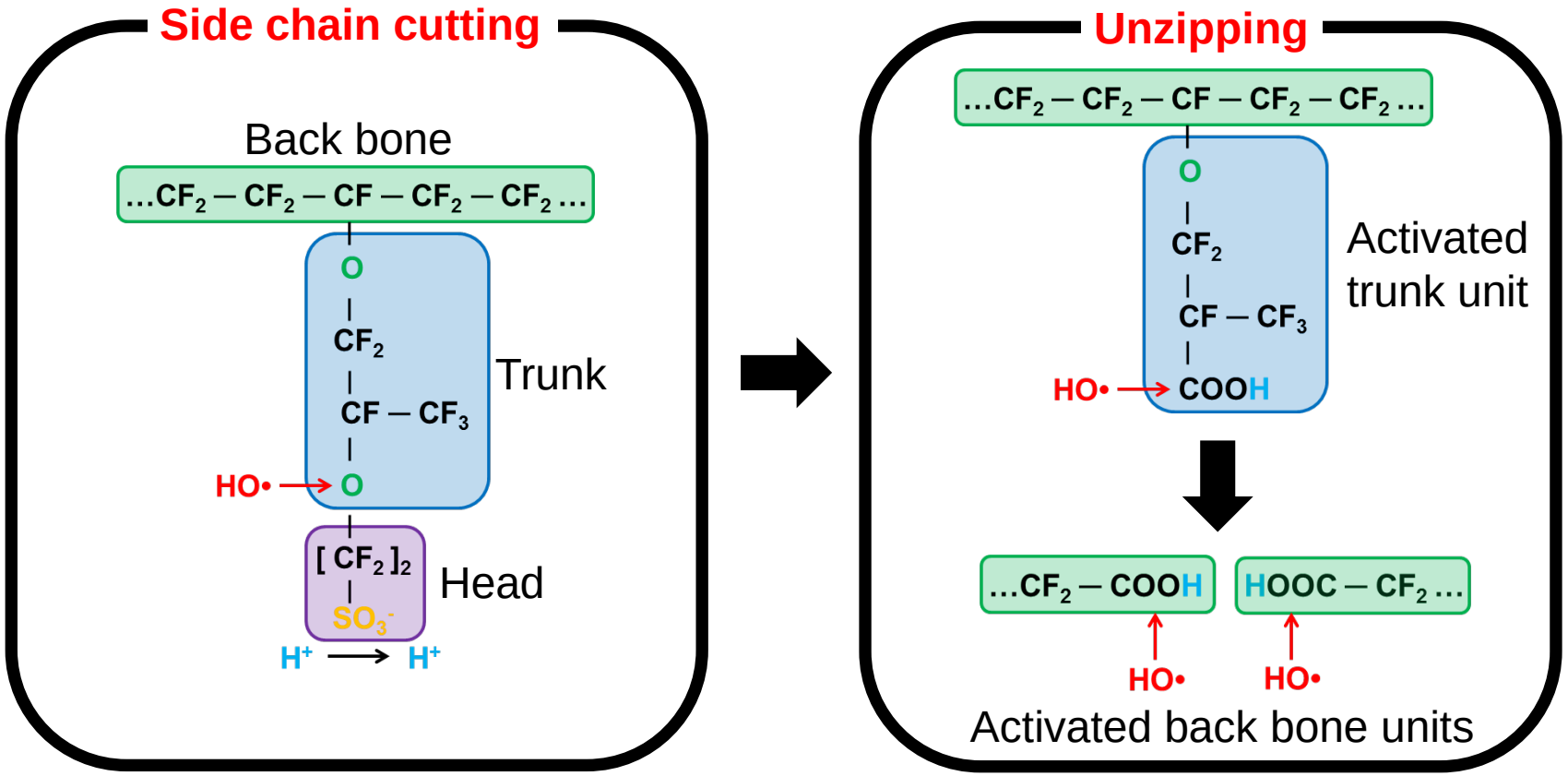

[1]: Ghelichi et al., **2014**, *J. Phys. Chem. B*, 118(38).

Degradation Reactions

Nr.	Reaction	k (M^{-1} s^{-1})	E_{act} (kJ mol^{-1})
10	HO• + head group → products	$3.7 \cdot 10^6$	???
11	HO• + activated trunk unit → products	$7.9 \cdot 10^5$	≈70
12	HO• + activated back bone unit → products	$7.9 \cdot 10^5$	≈70

Side-chain cutting

Unzipping

Rate constants at room temperature:

- Measured by: Dreizler & Roduner, **2012**, *Fuel Cells*, 12(1).

Activation energy for unzipping:

- Estimated by: Gubler et al., **2011**, *J. Electrochem. Soc.*, 158(7).

Catalyst degradation: Particle growth mechanism

- The loss of electrochemical active surface area (ECSA) at the cathode is mainly responsible for performance degradation
- Loss of ECSA is related to a growth of the platinum particles
- Different processes can contribute to the particle growth:
  - Ostwald ripening
  - Coalescence
- Key property for mathematical desciption: particle size distribution (PSD) *N*(*r*)
- Balance equation for PSD

$$\frac{\partial N(r,t)}{\partial t} + \frac{\partial}{\partial r}\left(N(r,t)\frac{\partial r}{\partial t}\bigg|_{Ostwald} \right) = \frac{\delta N(r,t)}{\delta t}\bigg|_{Coal}$$

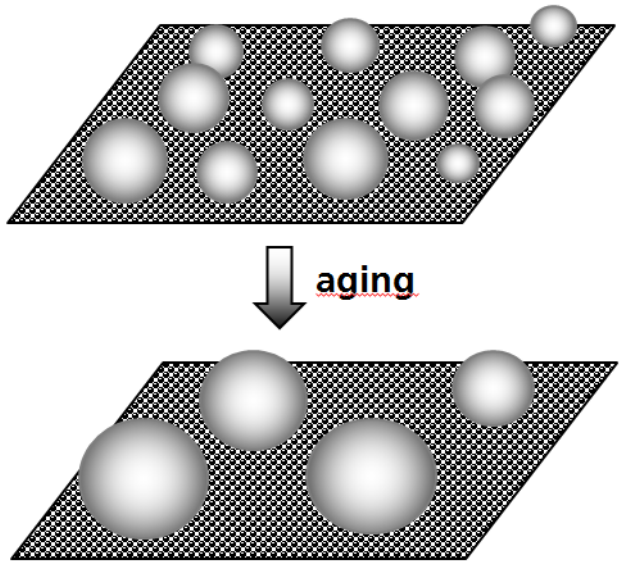

Catalyst degradation: Coalescence mechanism

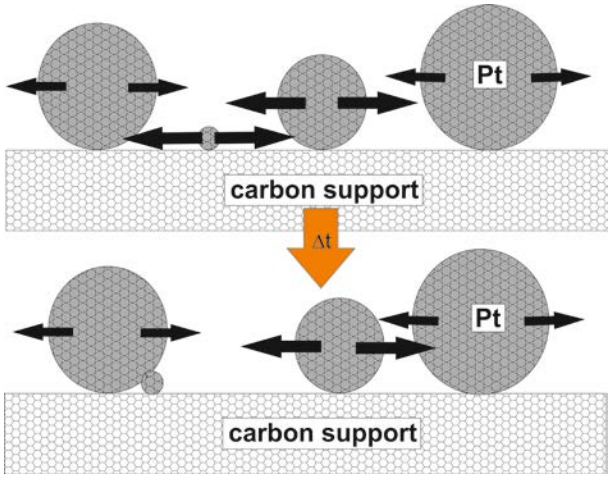

- Movement of the platinum particles on the carbon support can lead to coalescence of the particles
- The coalescence can be described by an integro-differential equation for the particle distribution:

$$\left.\frac{\delta N(r,t)}{\delta t}\right|_{Coal} = \underbrace{r^2 \int_0^r D(r')N(r',t)\frac{N((r^3-r'^3)^{1/3},t)}{(r^3-r'^3)^{2/3}}dr'}_{\text{Coalescence of two particles to one with size r}} - \underbrace{\int_0^\infty \big(D(r)+D(r')\big)N(r,t)N(r',t)dr}_{\text{Coalescence of a particle with size r}}$$

- Mechanisms for particle diffusion:
  - (i) Ion attachment/detachment[1]: $D(r) \sim r^{-1}$
  - (ii) Adatom diffusion[2] (high temp.): $D(r) \sim r^{-4}$

[1]: S.V. Khare, N.C. Bartelt, T.L. Einstein, *Physical Review Letters* 75 (1995) 2148
[2]: F. Behafarid, B.R. Cuenya, *Surface Science* 606 (2012) 908

Catalyst degradation: Ostwald ripening

- Change of particle sizes due to Pt dissolution and precipitation
  $Pt \rightleftarrows Pt^{2+} + 2\ e^-$
- The particle stability depends on the particle size (surface energy):

$$\Delta\mu_{GT} = \mu(r) - \mu(\infty) = \frac{2\Omega\gamma}{r}$$

- Experimental observation: Degradation is accelerated by cycling.
- Explanation: The formation and reduction of platinum oxides play an important role for the dissolution

→ A model for the oxide formation is needed

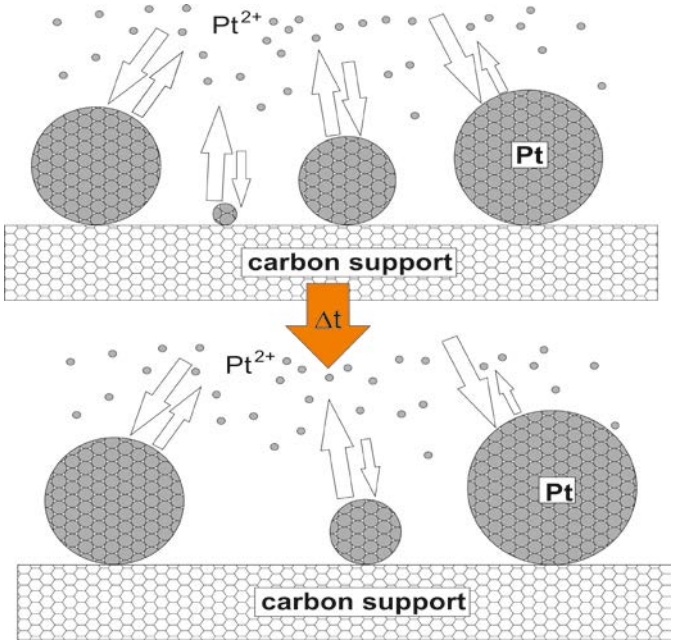

Catalyst degradation: Effect of platinum oxides

- Simple platinum oxide model:
  - Platinum oxides form a protective layer at high potentials, reducing the dissolution
    $Pt + H_2O \rightleftarrows PtO + 2H^+ + 2e^-$
  - At low potential the oxides are reduced
  - Going back to high potential leads to accelerated dissolution until the protective layer is formed again
    $Pt \rightleftarrows Pt^{2+} + 2\ e^-$

  →Fast degradation expected after sweep from low to high potential

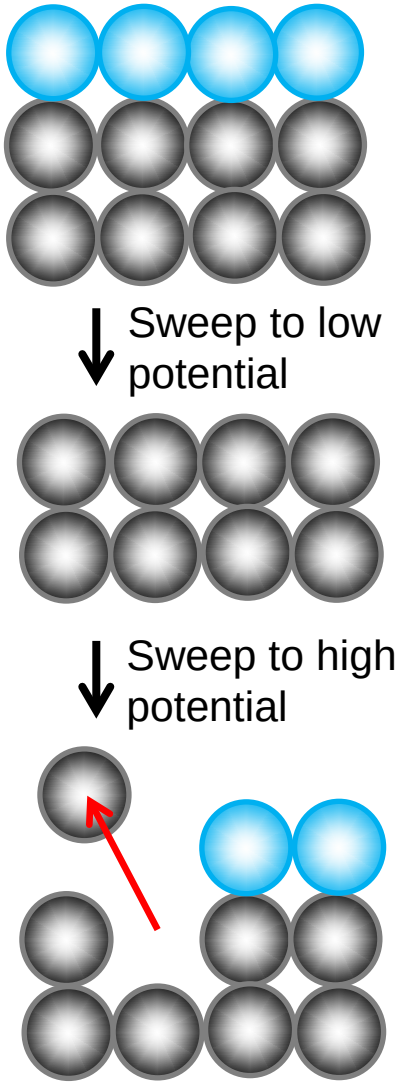

Catalyst degradation: Effect of platinum oxides

- Recent experiments show that faster dissolution occurs during sweep to low potentials [1] → contradiction to simple model!
- Advanced model:
  - Include the place exchange between platinum and oxygen atoms
    - $Pt + H_2O \rightleftarrows PtO_{surf} + 2H^+ + 2e^-$
    - $PtO_{surf} \rightleftarrows PtO_{bulk}$
    - $PtO_{bulk} + H_2O \rightleftarrows PtO_2 + 2H^+ + 2e^-$
  - Dissolution occurs also during the place exchange → accelerated degradation during sweep to low potentials
    - $PtO_{bulk} + 2\,H^+ \rightleftarrows Pt^{2+} + H_2O$

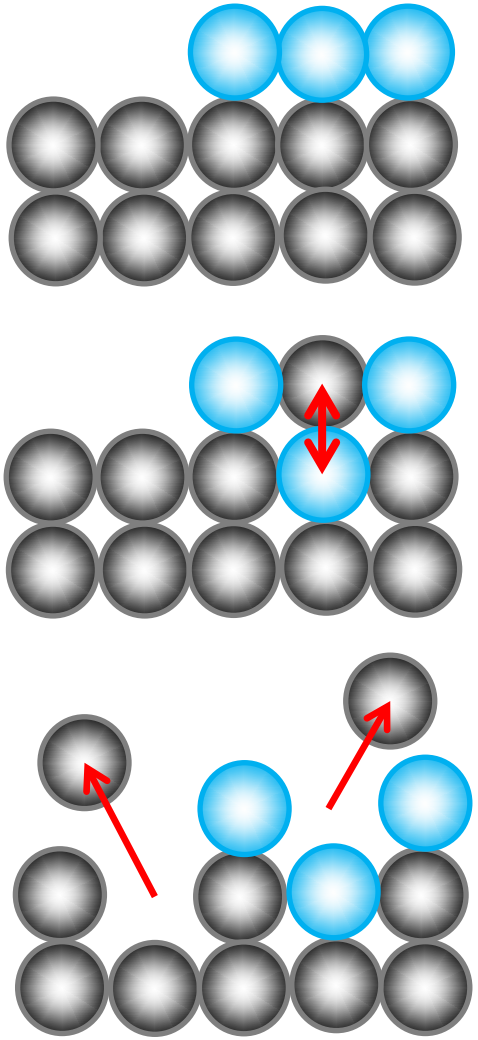

[1] A. A. Topalov et al., Chem. Sci. 5 (2014) 631

Catalyst degradation: Modeling the particle growth

- The particle growth mechanisms lead to a change in the PSD and a loss of ECSA
- Time evolution of ECSA depends on the mechanism

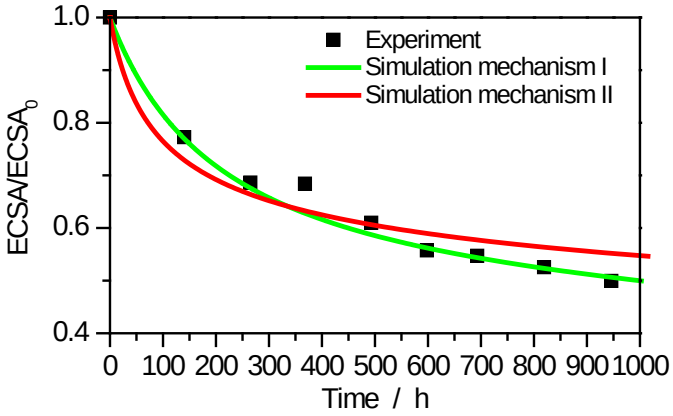

Catalyst degradation: Modeling the particle growth

- The particle growth mechanisms lead to a change in the PSD and a loss of ECSA
- Time evolution of ECSA depends on the mechanism
- The shape of the PSD also depends on the mechanism:
  - Tail at small particle sizes is formed during Ostwald ripening
  - Tail at large particle sizes and second peak is formed during coalescence

→Analyzing the PSD (e.g. with transmission electron microscopy) can help identifying the relevant degradation mechanism

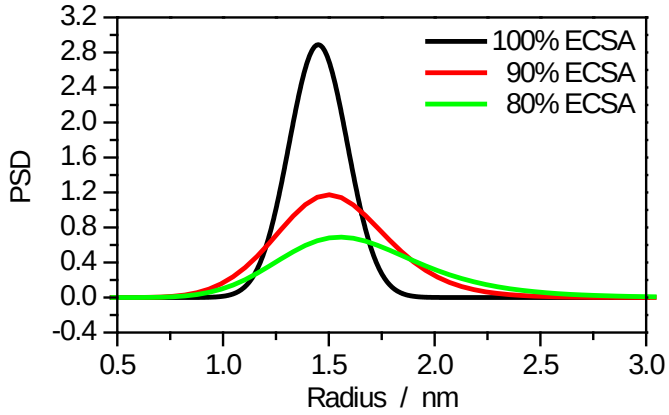

Ostwald ripening

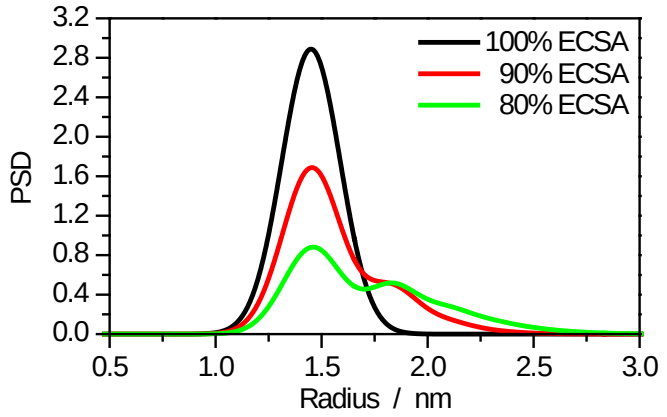

Coalescence